

用于锂硫电池高效硫载体的Co-N-C@KB 复合材料的规模化制备策略

陆小祥¹ 黎天宝² 涂飞跃² 李中良² 朱徐锟¹

孙 灿¹ 靳亚超¹ 宋 力^{*1} 张明道^{*1} 曹 晖^{*1}

(¹南京信息工程大学环境科学与工程学院,江苏省大气环境监测与污染控制重点实验室,
大气环境与装备技术协同创新中心,南京 210044)

(²长沙矿冶研究院有限公司,长沙 410012)

摘要: 硫正极较差的性能严重阻碍了锂硫电池的商业化进程,这些因素包括较低的导电能力以及在促进多硫化物转化方面较差的催化活性。我们开发了一种基于配体调控合成和低温热解的规模化策略来制备高效的正极复合材料(Co-N-C@KB),这种材料由富含Co-N-C活性位点的科琴黑(KB)组成。原子级分散的Co-N-C活性位点被证明有利于多硫化物在正极的转化,因而可以提高锂硫电池的容量和循环寿命。基于此,Co-N-C@KB作为正极可以使锂硫电池获得高达1 442 mAh·g⁻¹的初始放电容量,并且该电池在长时间的稳定性测试中具有出色的容量保持能力。

关键词: 锂硫电池;原子级分散的催化剂;碳材料;硫载体;吸附

中图分类号: O614.81*2; O613.71; O613.51 文献标识码: A 文章编号: 1001-4861(2021)06-1125-10

DOI: 10.11862/CJIC.2021.105

Scale-Up Strategy to Develop Highly-Effective Co-N-C@KB Composites as Sulfur Host for Lithium-Sulfur Battery

LU Xiao-Xiang¹ LI Tian-Bao² TU Fei-Yue² LI Zhong-Liang² ZHU Xu-Kun¹

SUN Can¹ JIN Ya-Chao¹ SONG Li^{*1} ZHANG Ming-Dao^{*1} CAO Hui^{*1}

(¹School of Environmental Science and Engineering, Nanjing University of Information Science & Technology,
Jiangsu Key Laboratory of Atmospheric Environment Monitoring and Pollution Control,

Collaborative Innovation Center of Atmospheric Environment and Equipment Technology, Nanjing 210044, China)

(²Changsha Research Institute of Mining and Metallurgy Co. Ltd, Changsha 410012, China)

Abstract: The commercialization process of Li-S battery is seriously impeded by the poor performance of sulfur cathode, including the low conductivity and dissatisfactory activity for facilitating the polysulfide conversion. In this work, we developed a scale-up method to synthesize an efficient cathode material (Co-N-C@KB) with abundant Co-N-C active sites on the Ketjen Black (KB), through a ligand-mediated-synthesis and a low-temperature-pyrolysis strategy. The uniformly distributed Co-N-C active sites were proved to be favorable for the conversion of polysulfide at the cathode, hence improving the capacity and cyclic life of Li-S battery. As a result, the Co-N-C@KB cathode for the Li-S battery could deliver an initial discharge specific capacity as high as 1 442 mAh·g⁻¹, and have the excellent capability for capacity retention during the long-term stability test.

Keywords: Li-S battery; atomically dispersed catalyst; carbon materials; sulfur host; adsorption

收稿日期: 2021-01-17。收修改稿日期: 2021-03-20。

国家自然科学基金(No.21905139, 51902166)资助。

*通信联系人。E-mail: songli@nuist.edu.cn, matchlessjimmy@163.com, jinyachao@nuist.edu.cn

0 Introduction

In recent years, lithium-sulfur (Li-S) battery has been praised as one of the most promising next-generation energy-storage systems, due to its prominent theoretical specific capacity (1 675 mAh·g⁻¹) and energy density (2 615 Wh·kg⁻¹)^[1-2]. The characteristics, including low cost, easily-acquired electrode materials and environmental friendliness give lithium-sulfur battery an obvious edge over other candidates in the fields of electronic devices, unmanned aerial vehicles and new energy vehicles^[3-5]. Although the theoretical energy density of Li-S battery has surpassed that of the conventional lithium-ion battery, the challenges at the sulfur cathode and lithium anode still hinder the industrial application of Li-S battery^[6-8]. Due to the low conductivity of sulfur and its reduction products (Li₂S/Li₂S₂), the utilization efficiency of active substances in Li-S batteries is low and it is difficult to reach the theoretical specific capacity^[9-10]. Besides, the charging and discharging processes at the sulfur cathode include multi-step redox reactions, and the appearance of soluble polysulfide will cause shuttle effect, leading to the low utilization rate of sulfur and shortening battery life^[11].

At present, fabricating sulfur-based cathodes with superior performance has become one of the main orientations to ameliorate the Li-S batteries. The most commonly used method is to embed sulfur into high specific-surface nanocarbon, including ordered mesoporous carbon, carbon nanotubes^[12-15], graphene^[16] and metal-organic-framework (MOF) derived carbon materials^[17-18]. Although excellent conductivity of these carbon materials evidently enhances the battery performance, weak physical interaction between nonpolar carbon and the polar lithium polysulfide still cannot block the occurrence of shuttle effect. In the subsequent studies, it was proved that some transition metals (Co^[19-21], Ni^[22-23] and Mo^[24-25]), especially atomically dispersed metal on the carbon matrix^[26-29], can be employed as the electrocatalysts for rapid conversion of polysulfide, which suppresses the shuttle effect and enhances the capacity of collecting polysulfide, therefore improving the cycling stability and capacity of Li-S bat-

teries. Based on this, Ma et al.^[30] synthesized a polysulfide mediator composed of nitrogen-doped carbon nanotube (N - CNT) forest planted on cobalt nanoflowers (N - CNTs/Co - NFs), used as an efficient sulfur host material for Li-S batteries. Li et al.^[31] synthesized a three-dimensional porous nitrogen-doped carbon polyhedron (Co/CoP@NC) and proved that the doping of Co transition metal exhibits strong chemisorption capacity with sulfur species and electrocatalytic effect for polysulfide conversion. Chen et al.^[32] developed a scalable process to prepare a composite with Co-nanoparticle-embedded and nitrogen-doped carbon nanotube/nano-polyhedra (Co-NCNT/NP) superstructures, which provides the idea for mass preparation of efficient sulfur host materials.

Inspired by these works, the carbon composite material coupled with uniformly dispersed transition metal atoms can be prepared and used as the effective sulfur host material at a very low cost. In this work, a ligand-mediated synthesis procedure was developed to capture the Co ions in the precursor, followed with a low-temperature-pyrolysis process, and this would result in uniformly dispersed Co-N-C sites on the carbon support. Via utilization of the cheap ligand of 2,2'-bipyridine, a close relationship can be built between the ligands and metal cations, which would lead to the formation of Co-N-C species supported on the carbon after the process of 600 °C pyrolysis. This strategy can effectively alleviate the agglomeration of Co. As a result, the composite materials possess excellent electrical conductivity benefited from the carbon support and strong catalytic activity derived from the Co-N-C sites. Compared with the conventional synthetic method, the Co-N-C@carbon supports (Ketjen Black (KB), carbon nanotube (CNTs) and Super P) can be synthesized in a large scale and with much less cost through this strategy. The abundant Co-N-C species in Co-N-C@KB were proved to be ultimately conducive to the adsorption and conversion of polysulfides. Due to the structural and componential merits, the Co-N-C@KB can be used as an effective S host in Li-S batteries and demonstrate remarkable battery performance.

1 Experimental

1.1 Synthesis of Co-N-C@KB

In order to synthesize Co-N-C@KB, cobalt(II) acetate (708 mg, $177.02 \text{ g}\cdot\text{mol}^{-1}$) and 2, 2'-bipyridine (1 874 mg, $156.19 \text{ g}\cdot\text{mol}^{-1}$) were firstly dissolved in 94 mL of ethanol, followed with stirring at $40 \text{ }^\circ\text{C}$ for 12 h. Secondly, KB (3 873 mg) was added to the solution and heated at $60 \text{ }^\circ\text{C}$ for 6 h in an oil bath under continuous magnetic agitation. The obtained dispersion was heated at $80 \text{ }^\circ\text{C}$ for 12 h to vaporize the ethanol until black powders were formed. The black powders were lightly ground with a mortar and pestle, and then transferred to an alumina crucible and placed in a tubular furnace. The furnace was therewith heated to $600 \text{ }^\circ\text{C}$ at a speed of $10 \text{ }^\circ\text{C}\cdot\text{min}^{-1}$ under Ar protection and then remained at $600 \text{ }^\circ\text{C}$ for 2 h to get the carbonized product Co-N-C@KB. The procedures of synthesizing Co-N-C@CNTs and Co-N-C@Super P were similar to Co-N-C@KB except for the replacement of KB with CNTs or Super P.

1.2 Synthesis of Co-N-C@KB/S

Co-N-C@KB as well as the sublimated sulfur powders with the mass ratio of 2:7 was milled for 15 min in order to receive a homogeneous mixture. Next, the powder mixture was placed in the quartz tube and an annealing process was carried out in an argon atmosphere. The mixture was heated at $115 \text{ }^\circ\text{C}$ for 30 min and then heated at $155 \text{ }^\circ\text{C}$ for 12 h ($2 \text{ }^\circ\text{C}\cdot\text{min}^{-1}$) to obtain the Co-N-C@KB/S powder. Co-N-C@Super P/S, Co-N-C@CNTs/S, KB/S, Super P/S and CNTs/S composites were prepared in a similar approach.

1.3 Lithium polysulfide adsorption study

First, an appropriate amount of sublimated sulfur and lithium sulfide (Li_2S) (molar ratio of 5:1) were dissolved in 1, 3-dioxolane (DOL) and 1, 2-dimethoxyethane (DME) (1:1, V/V) solution and stirred on a magnetic mixer for 24 h to obtain a $2 \text{ mmol}\cdot\text{L}^{-1}$ polysulfide solution. 20 mg of Co-N-C@KB was added to 4.0 mL polysulfide solution, and then the resulting mixture was vigorously stirred for 2 h and aged for 12 h. The sample status during the experiment was recorded.

1.4 Cells assembly and tests

The active material Co-N-C@KB/S and polyvinyl-

dene fluoride (PVDF) were ground at a mass ratio of 9:1 together with *N*-methyl pyrrolidone (NMP) to obtain an ink. The ink was then coated on aluminum foil and dried at $80 \text{ }^\circ\text{C}$ for 12 h. Afterwards, the active-material-coated aluminum foil was cut into small wafers, with the area of 1.13 cm^2 . The area loading of S was between 1.5 and $2.0 \text{ mg}\cdot\text{cm}^{-2}$; the electrolyte on a single cell was about $60 \text{ }\mu\text{L}$. The battery was assembled in the form of 2032 coin-shaped cells, in which lithium metal foil was employed as the anode, with Celgard 2400 as the diaphragm and $1 \text{ mol}\cdot\text{L}^{-1}$ $\text{LiN}(\text{CF}_3\text{SO}_2)_2$ (LiTFSI) in DME+DOL (1:1, V/V) with LiNO_3 (mass fraction of 2%) as the electrolyte. All the battery assembling procedures were carried out in a glove box with less than 10^{-7} moisture and oxygen and the battery performance was evaluated by a LAND test system (Wuhan LAND Electronics Co., Ltd.). Cyclic voltammetry (CV) and AC impedance (EIS) were performed on CHI660E electrochemical workstation, with the sweep velocity of $0.1 \text{ mV}\cdot\text{s}^{-1}$ and the test voltage range of 1.7~2.8 V. EIS test ranged from 0.01 to 100 kHz with an amplitude of 10 mV.

1.5 Characterizations of material

The crystal structure and phase composition of the obtained materials were tested by X-ray diffraction (XRD) using a Shimadzu X-ray diffractometer (XRD-6000) with the Cu $K\alpha$ radiation ($\lambda = 0.154 \text{ nm}$). The working current was 20 mA and working voltage was 40 kV with 2θ range of $10^\circ\sim 80^\circ$. The morphology and microstructure of the materials were observed through scanning electron microscope (SEM, Quanta FEC 250, 10 kV), and transmission electron microscopy (TEM, JEM-1400plus, 100 kV) appliances. The S content was measured by a thermal analyzer (Setaram Labsys Evo) in an N_2 atmosphere with a heating rate of $10 \text{ }^\circ\text{C}\cdot\text{min}^{-1}$ from room temperature to $600 \text{ }^\circ\text{C}$. Specific surface area and pore size distribution were tested by a specific surface analyzer (SA3100, Beckman Coulter). The elemental and chemical state information were analyzed with the X-ray photoelectron spectroscopy (XPS, AXIS-Ultra DLD). Raman spectroscopy was evaluated using the Renishaw inVia spectrometer.

1.6 Soft package battery assembly

The working electrode was made of active materials (Co-N-C@KB/S), KB and polymer binder (polytetrafluoroethylene, PTFE) in a weight ratio of 80:10:10. Ethanol was used as a solvent and added into the above mixture, for the formation of a black paste. The paste was coated onto an aluminum mesh to form an S-cathode, which was then dried at 80 °C for 12 h under the vacuum condition. The S-cathode and Li-anode were folded to form multideck electrodes in an Ar-protected glove box. Then, aluminum-plastic shells were used to pack the stacked electrodes. After that, electrolyte was added inside the battery through a vacuum injection machine. The electrolyte contains 1 mol·L⁻¹ LiTFSI in DME+DOL (1:1, V/V) with LiNO₃ (mass fraction of 2%). The mass ratio of electrolyte and sulfur was 4. At last, the aluminum plastics shells outside the electrodes were sealed by a heat-sealing device.

2 Results and discussion

2.1 Structure characterization

The synthesis path of Co-N-C@KB/S is illustrated in Fig.1. First, uniformly dispersed 2,2'-bipyridine was used as a ligand, combining with cobalt(II) acetate to form a metal complex, which would be absorbed on the KB. The surface-modified carbon was further pyrolyzed in argon at 600 °C to immobilize the Co species, lead-

ing to the production of Co-N-C@KB. Actually, with this method, a series of sulfur host materials with Co-N-C species on the carbon supports can be synthesized. The significant effect of Co-N-C@KB on anchoring of polysulfide can be proved by the adsorption test as exhibited in Fig.S1. Compared with the result of pure KB, a distinct adsorption phenomenon was found when Co-N-C@KB was added into the solution of Li₂S_n. This result indicates the strong adsorbing capability of Co-N-C@KB to capture lithium polysulfide.

Physical and chemical characterization were used to reveal the structural and morphological characteristics. The morphologies of the three samples were characterized by SEM (Fig. 2a~2c), wherein there were no obvious particles present on the three carbon supports. There were similar morphologies for Co-N-C@KB and Co-N-C@Super P. Co-N-C@CNTs exhibited uniformly distributed tubes, which construct a multi-dimensional network, improving the electrical conductivity of the material and speeding up the transport of ions and electrons. The further analysis of the microstructure was characterized by TEM (Fig. S2a~S2c). The scanning transmission electron microscope (STEM) image and the EDS elemental mappings of Co-N-C@KB are demonstrated in Fig.2d and 2e, wherein Co, N and O were homogeneously incorporated in the carbon support, illustrating that the carbon composites containing uni-

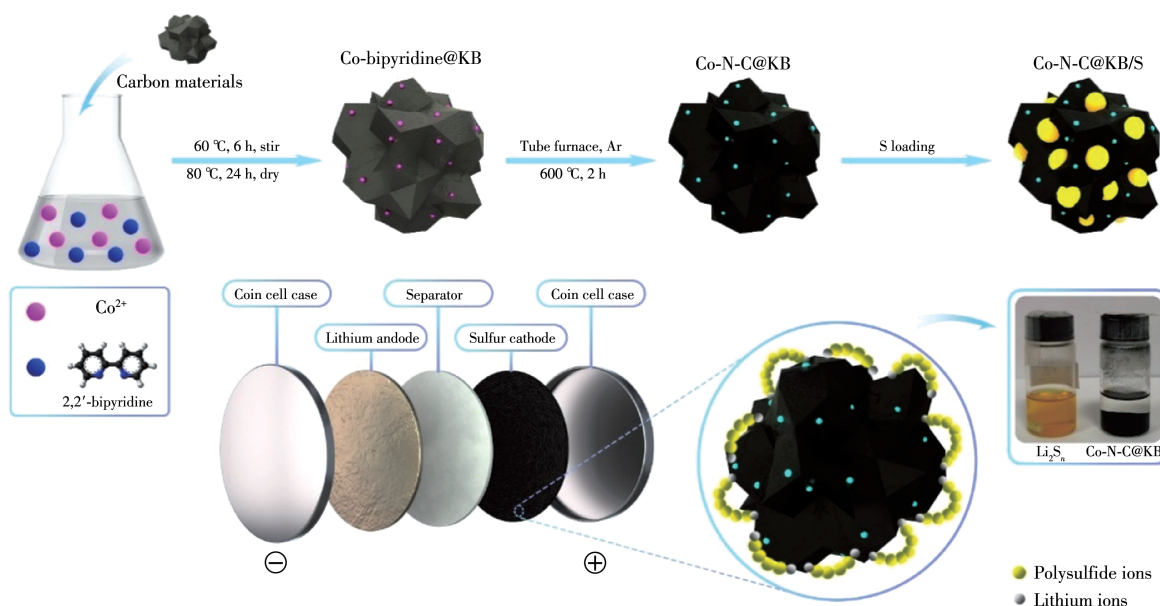


Fig.1 Schematic illustration of synthesis process and adsorption mechanism for Co-N-C@KB/S composite

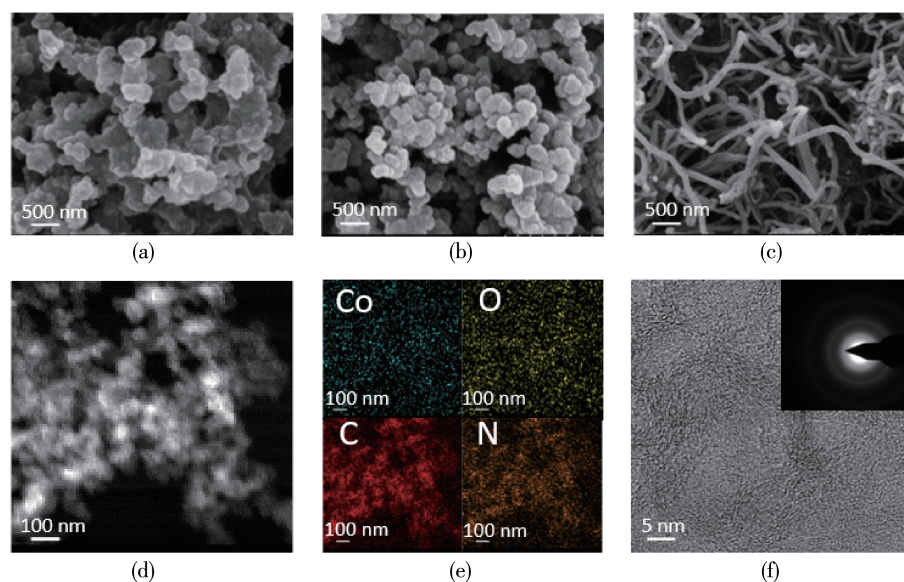


Fig.2 SEM images of (a) Co-N-C@KB, (b) Co-N-C@Super P and (c) Co-N-C@CNTs; (d) STEM image of Co-N-C@KB and (e) corresponding EDS elemental mappings; (f) HRTEM image and SEAD pattern (inset) of Co-N-C@KB

fomly distributed Co-N-C species were successfully prepared. As can be exhibited through the high-resolution TEM (HRTEM) image of Co-N-C@KB in Fig.2f, there was no crystalline lattice fringe present in the carbon support and the selected area electron diffraction (SAED) pattern (inset) showed no rings or bright spots, indicating very low crystallinity and no Co agglomeration. These results indicate that the Co-N-C were uniformly dispersed on the KB support.

The XRD patterns of Co-N-C@KB, Co-N-C@Super P, Co-N-C@CNTs and KB are displayed in Fig.3a. It can be found that the broad peaks centered at around 24° and 44° correspond to the (002) and (100) planes of graphitic carbon. No metal-related peaks were observed in the XRD patterns, which is consistent with the TEM results. This result indicates that a low pyrolysis temperature of 600°C prevents the formation of metal nanoclusters. Raman spectra are shown in Fig. 3b, wherein two significant carbon peaks at 1341 cm^{-1} (D band) and 1597 cm^{-1} (G band) correspond to the defective and graphitic structure, respectively. The I_D/I_G values of Co-N-C@KB and KB were 1.067 and 1.197, respectively, indicating the transformation of more amorphous carbon into graphitized carbon and ensuring the excellent conductivity of Co-N-C@KB. Nitrogen adsorption-desorption isotherms were collected to ana-

lyze the BET (Brunauer-Emmett-Teller) data of the composite, from which the pore-size distribution plots can be calculated with the Barrett-Joyner-Halenda (BJH) model. As shown in Fig. S3, all three samples showed the typical characteristics of high porosity. The BET specific surface areas of Co-N-C@KB, Co-N-C@Super P and Co-N-C@CNTs were calculated to be 195, 60 and $226\text{ m}^2\cdot\text{g}^{-1}$, respectively. Noticeably, the high specific surface areas of Co-N-C@KB would efficiently improve the capability of ion exchange with electrolyte and adsorption for polysulfide, thus contributing to its outstanding discharge specific capacity and cycling stability. TGA (thermogravimetric analysis) test was carried out to measure the sulfur ratio in the S/C composite, thus verifying the hosting capability of the materials to sulfur. The TGA results of Co-N-C@KB, Co-N-C@Super P and Co-N-C@CNTs are shown in Fig. S4. The sample began to lose weight at about 200°C , and the most obvious weight-loss phenomenon appeared at about 300°C , indicating that a large amount of S in the sample escaped at this step. The S contents of Co-N-C@KB, Co-N-C@Super P and Co-N-C@CNTs samples were determined to be mass fraction of 72.0%, 72.5% and 75.4% respectively, which are similar to the actual ratio of additions in the mixture. This result indicates that there was little S loss in the melting process and

the Co-N-C modified carbon composites had a strong affinity to S.

XPS analysis was used to further characterize the elemental composition of the samples. Fig.3c shows the XPS survey spectra of Co-N-C@KB, Co-N-C@Super P and Co-N-C@CNTs, indicating that the four elements of Co, C, N and O are successfully incorporated in the carbon support. This result is in keeping with the EDS spectrum as displayed in Fig. S5. The Co contents in Co-N-C@KB, Co-N-C@Super P and Co-N-C@CNTs are displayed in Table S1, wherein the Co content of Co-N-C@KB was calculated to be atomic fraction of 0.58%. Fig.3d exhibits the Co2p spectrum at the core

level, wherein there were six peaks, matched to Co2p_{3/2}, Co2p_{1/2} and satellite peaks, respectively. The peaks at 803.5, 796.2 and 792.1 eV correspond to the vibrating satellite peaks, Co²⁺ and Co³⁺ for Co2p_{1/2}, and the other three peaks at 786.5, 781.1 and 779.4 eV correspond to the vibrating satellite peaks, Co²⁺ and Co³⁺ for Co2p_{3/2}^[14]. As displayed in Fig.S6, the XPS spectra of Co-N-C@Super P and Co-N-C@CNTs demonstrate similar results to that of Co-N-C@KB. The C1s spectrum of Co-N-C@KB is shown in Fig. 3e, wherein the main peak at 284.8 eV can be fitted to the typical C=C bond. In addition to the C=C bond, the peak at 290.4 eV matches the C—O bond, which might be derived

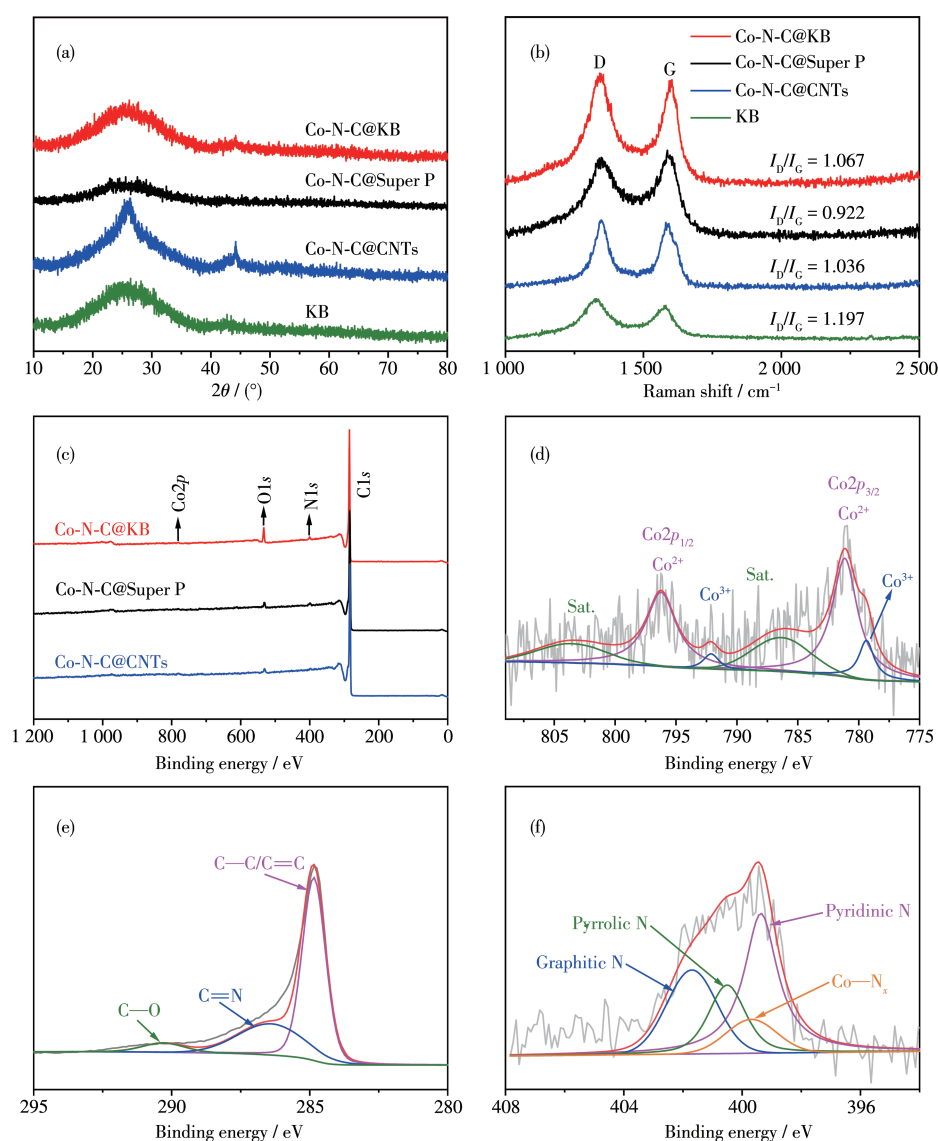


Fig.3 (a) XRD patterns and (b) Raman spectra of Co-N-C@KB, Co-N-C@Super P, Co-N-C@CNTs and KB; (c) XPS spectra of Co-N-C@KB, Co-N-C@Super P and Co-N-C@CNTs; (d-f) Co2p, C1s and N1s XPS spectra of Co-N-C@KB

from the partial oxidation of C in the air. The N1s spectrum of Co-N-C@KB is shown in Fig.3f, in which the peaks at 401.7, 400.5, 399.6 and 399.4 eV correspond to graphitic-N, pyrrolic-N, Co-N_x and pyridinic-N, respectively^[33]. The abundant Co-N_x and pyridinic-N would be helpful for the anchoring and conversion of the polysulfide^[6]. In addition, the O1s spectrum was provided in Fig.S7, which shows two peaks at the binding energies of 532.9 and 534.5 eV, indicating the presence of oxygen ions in the Co-N-C@KB^[34].

2.2 Electrochemical performance

The initial discharge/charge curves for Co-N-C@KB, Co-N-C@Super P, Co-N-C@CNTs, KB, Super P

and CNTs at 0.05C are shown in Fig.4a. The specific discharge capacities of Co-N-C@KB, Co-N-C@Super P and Co-N-C@CNTs were 1 216, 974 and 1 180 mAh·g⁻¹ respectively, greater than that of KB, Super P and CNTs under the same condition. This result shows that the introduction of Co-N-C species on the carbon efficiently increases the reaction sites and enlarges the capacity of Li-S battery. The EIS spectra of Co-N-C@KB and KB are shown in Fig.4b, to study the electron and ion transfer ability on the electrode interface. The charge-transfer resistance (R_{ct}) of Co-N-C@KB in the high-frequency region was about 120 Ω, much less than that of KB, indicating Co-N-C@KB has a faster

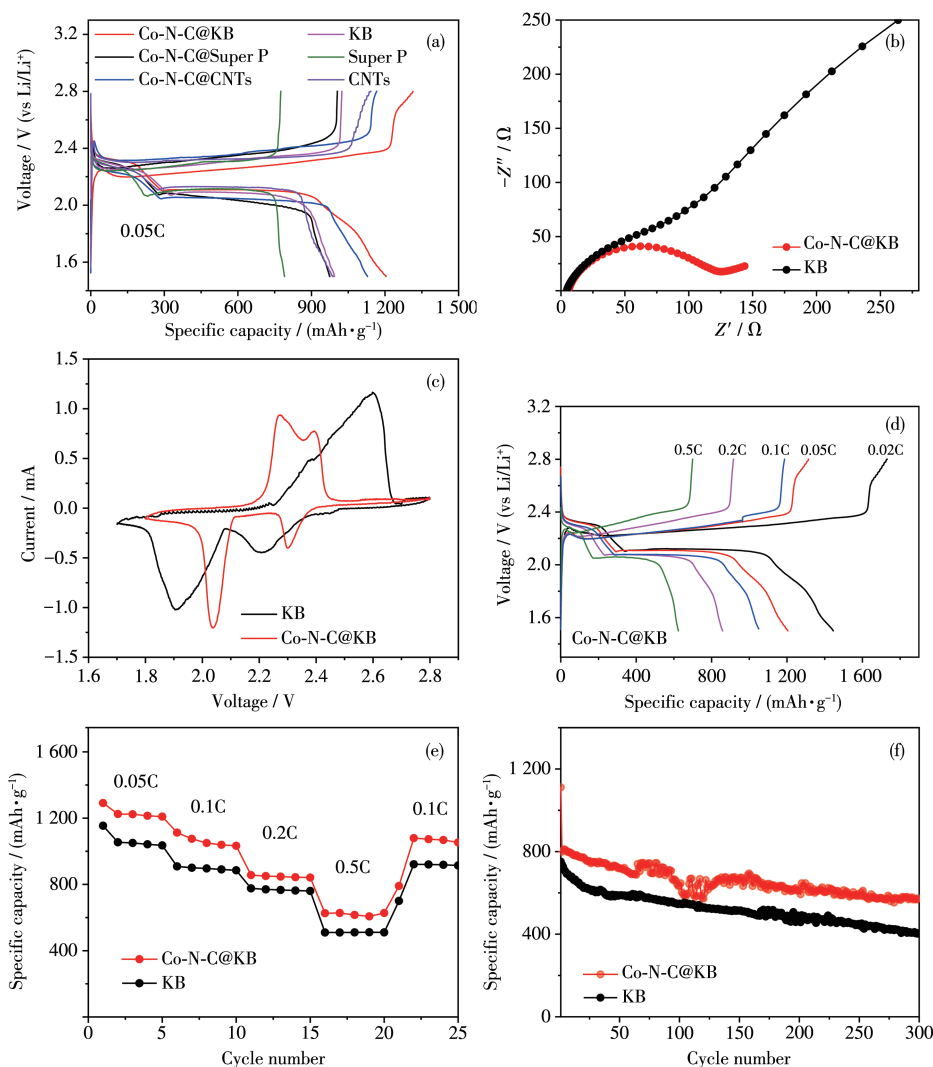


Fig.4 (a) Charge/discharge profiles of Co-N-C@KB, Co-N-C@Super P, Co-N-C@CNTs, KB, Super P and CNTs at 0.05C; (b) EIS spectra of Co-N-C@KB and KB; (c) CV curves of Co-N-C@KB and KB; (d) Charge/discharge profiles of Co-N-C@KB electrode at different current rates; (e) Rate capacities comparison between Co-N-C@KB and KB; (f) Cyclic performances of Co-N-C@KB and KB at 0.2C

charge transfer rate on the cathode/electrode interface, indicating superior reaction kinetics to KB. The CV curves of Co-N-C@KB and KB electrodes were performed within the voltage range of 1.7~2.8 V at 0.1 $\text{mV}\cdot\text{s}^{-1}$. As shown in Fig.4c, there were a couple of cathodic reduction peaks, as well as a couple of anodic oxidation peaks appearing at the symmetrical positions. For the Co-N-C@KB electrode, the reduction peak at about 2.32 V corresponds to the transition of S_8 into long-chain polysulfide (Li_2S_x , $4 \leq x \leq 8$), and another peak at around 2.03 V corresponds to the conversion of the long-chain polysulfide into short-chain Li_2S and Li_2S_2 ^[35]. The two anodic peaks at 2.27 and 2.39 V correspond to the oxidation of short-chain $\text{Li}_2\text{S}_2/\text{Li}_2\text{S}$ to polysulfides and then to elemental sulfur^[14]. Compared with the KB electrode, the Co-N-C@KB electrode undergoes distinguishable positive shift in the two cathodic peaks and remarkable negative shift in the anodic peaks. It is demonstrated that Co-N-C@KB can greatly decrease the electrochemical polarization and facilitate the polysulfide redox reaction kinetics. This result is consistent with the charge and discharge profiles in Fig.4a and indicates better transformation ability of discharge/charge products on the Co-N-C@KB electrode. To eval-

uate the rate capability, we ran the Co-N-C@KB-based Li-S batteries under progressively enlarged current rates, ranging from 0.02C to 0.5C. The related charge/discharge profiles are shown in Fig.4d, wherein the corresponding specific capacity recorded at 0.02C, 0.05C, 0.1C, 0.2C and 0.5C were 1 442, 1 216, 1 049, 858 and 623 $\text{mAh}\cdot\text{g}^{-1}$, respectively. Furthermore, the discharge capacities obtained at various current densities during the cycling discharge/charge tests were plotted as demonstrated in Fig.4e, indicating that larger capacities at all the four current densities were achieved by Co-N-C@KB, compared with KB. When the current density returned to 0.1C, the specific capacity of the Co-N-C@KB-based battery recovered to 1 059 $\text{mAh}\cdot\text{g}^{-1}$, with a retention rate of nearly 95%, indicating a good rate capability of the Co-N-C@KB electrode. The cyclic stabilities of Co-N-C@KB and KB were evaluated through a galvanostatic cyclic discharging/charging process at the current density of 0.2C. As shown in Fig.4f, the Co-N-C@KB-based Li-S battery showed a stable charge/discharge reversibility with a capacity retention rate of more than 72.5% up to 300 cycles. It was found that the Co-N-C@KB-based battery has higher retention rate of the discharge capacity in the whole

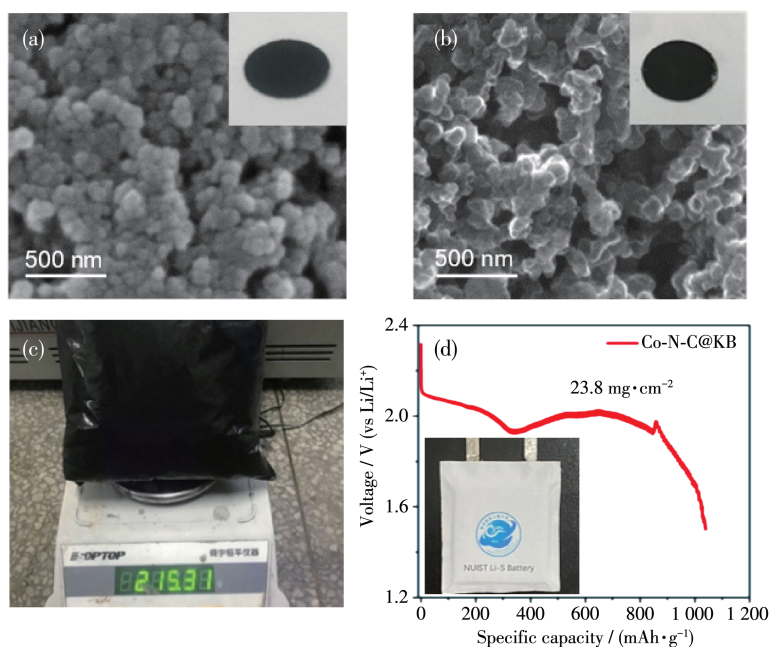


Fig.5 SEM images of Co-N-C@KB (a) before and (b) after 300 discharge/charge cycles; (c) Digital photograph for Co-N-C@KB synthesized in large scale; (d) Discharge curve and digital image (inset) of Co-N-C@KB-based soft-pack Li-S battery

300 cycles in comparison with that of the KB-based counterpart. These results show that Co-N-C@KB can effectively facilitate the conversion of polysulfide and enhance the effective utilization of the cathode S, thus improving the discharge depth. For comparison, some reported transition metals-based carbon materials as the sulfur hosts and their related electrochemical performances are listed in Table S2^[36-45]. Compared with the reported materials, the material in this work has some advantages in the initial discharge performance and cycle performance.

The SEM images of Co-N-C@KB electrode before and after 300 discharge/charge cycles are given in Fig.5a and 5b. There was no obvious change in the morphology of the KB particles. This result demonstrates the structural stability of Co-N-C@KB for the reversible charge-discharge processes. Fig.5c shows the mass-preparation scale of Co-N-C@KB composite can be up to over 215 g for 10-time repetitive preparing procedures. As shown in Fig.5d, the mass of as-synthesized active Co-N-C@KB composite is enough for preparing the necessary cathode material of a soft-package Li-S battery (with a high surface loading of 23.8 mg·cm⁻² on the cathode), whose size diagram is shown in Fig.S8. This battery can deliver a discharge capacity of 621 mAh and achieve a specific capacity of 1 042 mAh·g⁻¹, indicating a potential for the application in high-capacity and large-size Li-S batteries.

3 Conclusions

To sum up, through utilizing the cost-effective ligand 2, 2'-bipyridine, a series of Co-N-C@carbon composites can be prepared. Specially, the Co-N-C@KB electrode combines the high conductivity, the high specific surface area of KB and abundant functional sites of Co-N-C species. The rich surface defects and active sites in Co-N-C@KB help to anchor the polysulfide and therewith catalyze its conversion, thus not only enhancing the utilization efficiency of S but also effectively inhibiting the shuttle effect. Due to the above advantages, the Co-N-C@KB electrode helps the Li-S battery to achieve a high initial capacity of 1 442 mAh·g⁻¹ and excellent capability of capacity retention

during the cyclic discharge/charge process. In addition, this method could be applied to various kinds of transition metals, which can be effectively and uniformly supported on the carbon matrix. Therefore, this work paved a simple and economical way by modifying the conductive carbon materials with abundant transition metal atoms as the active sites to improve the performance of the chargeable Li-S battery.

Supporting information is available at <http://www.wjhxxb.cn>

Declaration of interests: The authors declare that there are no known competing financial interests or personal relationships that could have appeared to influence the work reported in this paper.

Acknowledgments: This work was funded by grants from the National Natural Science Foundation of China (Grants No.21905139, 51902166). Meanwhile, this work was supported by Jiangsu Cyan Engineering of Higher Education, Priority Academic Program Development of Jiangsu Higher Education Institutions (PAPD), Jiangsu Joint Laboratory of Atmospheric Pollution Control, and Jiangsu Engineering Technology Research Center of Environmental Cleaning Materials. SONG Li and JIN Ya-Chao were financially supported by Research Start-up Fund of NUIST.

References:

- [1] Fang R P, Zhao S Y, Sun Z H, Wang D W, Cheng H M, Li F. *Adv. Mater.*, **2017**,**29**:1-25
- [2] Li G R, Wang S, Zhang Y N, Li M, Chen Z W, Lu J. *Adv. Mater.*, **2018**,**30**:1-19
- [3] Liu X, Huang J Q, Zhang Q, Mai L Q. *Adv. Mater.*, **2017**,**29**:1601759
- [4] Zang Y, Pei F, Huang J H, Fu Z H, Xu G, Fang X L. *Adv. Energy Mater.*, **2018**,**8**(31):1802052
- [5] Bai S Y, Liu X Z, Zhu K, Wu S C, Zhou H S. *Nat. Energy*, **2016**,**1**(7):1-6
- [6] Zeng P, Chen M F, Jiang S X, Li Y F, Xie X, Liu H, Hu X Y, Wu C, Shu H B, Wang X Y. *ACS Appl. Mater. Interfaces*, **2019**,**11**(25):22439-22448
- [7] Xua Z L, Kimb J K, Kang K. *Nano Today*, **2018**,**19**:84-107
- [8] Ye H L, Li M, Liu T C, Li Y G, Lu J. *ACS Energy Lett.*, **2020**,**5**(7):2234-2245
- [9] Zhu X, Ye J W, Lu Y F, Jia X L. *ACS Sustainable Chem. Eng.*, **2019**,**7**(13):11241-11249
- [10] Mi Y Y, Liu W, Wang Q, Jiang J B, Brudvig G W, Zhou H H, Wang H L. *J. Mater. Chem. A*, **2017**,**5**(23):11788-11793

- [11] Papandrea B, Xu X, Xu Y X, Chen C Y, Lin Z Y, Wang G M, Luo Y Z, Liu M, Huang Y, Mai L Q, Duan X F. *Nano Res.*, **2016**,**9**(1):240-248
- [12] 潘沛锋, 陈平, 方亚男, 单淇, 陈宁娜, 冯晓苗, 刘瑞卿, 李盼, 马延文. *无机化学学报*, **2020**,**36**(3):575-583
- PAN P F, CHEN P, FANG Y N, SHAN Q, CHEN N N, FENG X M, LIU R Q, LI P, MA Y W. *Chinese J. Inorg. Chem.*, **2020**,**36**(3):575-583
- [13] Lu C X, Lu C, Xiao D J, Chen C M, Yuan S X. *Energy Storage Mater.*, **2018**,**10**:216-222
- [14] Zhao S Y, Tian X H, Zhou Y K, Ma B, Natarajan A. *J. Energy Chem.*, **2020**,**46**:22-29
- [15] Luo L Y, Qin X Y, Wu J X, Liang G M, Li Q, Liu M, Kang F Y, Chen G H, Li B H. *J. Mater. Chem. A*, **2018**,**6**(18):8612-8619
- [16] 杨孝昆, 陈阿玲, 易清风. *无机化学学报*, **2021**,**37**(1):157-170
- YANG X K, CHEN A L, YI Q F. *Chinese J. Inorg. Chem.*, **2021**,**37**(1):157-170
- [17] Fang R P, Chen K, Yin L C, Sun Z H, Li F, Cheng H M. *Adv. Mater.*, **2019**,**31**(9):1-22
- [18] Zhang M D, Dai Q B, Zheng H G, Chen M D, Dai L M. *Adv. Mater.*, **2018**,**30**(10):1-10
- [19] Pei F, Fu A, Ye W B, Peng J, Fang X L, Wang M S, Zheng N F. *ACS Nano*, **2019**,**13**(7):8337-8346
- [20] Chen T, Zhang Z W, Cheng B R, Chen R P, Hu Y, Ma L B, Zhu G Y, Liu J, Jin Z. *J. Am. Chem. Soc.*, **2017**,**139**(36):12710-12715
- [21] Chen T, Ma L B, Cheng B R, Chen R P, Hu Y, Zhu G Y, Wang Y R, Liang J, Tie Z X, Liu J, Jin Z. *Nano Energy*, **2017**,**38**:239-248
- [22] Fu A, Wang C Z, Pei F, Cui J Q, Fang X L, Zheng N F. *Small*, **2019**,**15**(10):1-21
- [23] Yang H Z, Shang L, Zhang Q H, Shi R, Waterhouse G I N, Gu L, Zhang T R. *Nat. Commun.*, **2019**,**10**(1):4585
- [24] Lin H B, Yang L Q, Jiang X, Li G C, Zhang T R, Yao Q F, Zheng G Y W, Lee J Y. *Energy Environ. Sci.*, **2017**,**10**(6):1476-1486
- [25] Hao Q Y, Cui G L, Zhang Y G, Li J D, Zhang Z S. *Chem. Eng. J.*, **2020**,**381**:122672
- [26] Liu X C, Zhou S P, Liu M, Xu G L, Zhou X D, Huang L, Sun, S G, Amine K, Ke F S. *Nano Energy*, **2018**,**50**:685-690
- [27] 胡青桃, 张文达, 李涛, 晏晓东, 顾志国. *无机化学学报*, **2020**,**36**(8):1573-1581
- HU Q T, ZHANG W D, LI T, YAN X D, GU Z G. *Chinese J. Inorg. Chem.*, **2020**,**36**(8):1573-1581
- [28] Lu X L, Zhang Q F, Wang J, Chen S H, Ge J M, Liu Z M, Wang L L, Ding H B, Gong D C, Yang H G, Yu X Z, Zhu J. *Chem. Eng. J.*, **2019**,**358**:955-961
- [29] Ma L B, Zhang W J, Wang L, Hu Y, Zhu G Y, Wang Y R, Chen R P, Chen T, Tie Z X, Liu J, Jin Z. *ACS Nano*, **2018**,**12**(5):4868-4876
- [30] Ma L B, Lin H N, Zhang W J, Zhao P Y, Zhu G Y, Hu Y, Chen R P, Tie Z X, Liu J, Jin Z. *Nano Lett.*, **2018**,**18**(12):7949-7954
- [31] Li Y J, Xu P, Chen G L, Mou J R, Xue S F, Li K, Zheng F H, Dong Q F, Hu J H, Yang C H, Liu M L. *Chem. Eng. J.*, **2020**,**380**:122595
- [32] Chen T, Cheng B R, Zhu G Y, Chen R P, Hu Y, Ma L B, Lv H L, Wang Y R, Liang J, Tie Z X, Jin Z, Liu J. *Nano Lett.*, **2017**,**17**(1):437-444
- [33] Park S K, Lee J K, Kang Y C. *Adv. Funct. Mater.*, **2018**,**28**(18):1-9
- [34] Fu J, Kang W B, Guo X D, Wen H, Zeng T B, Yuan R X, Zhang C H. *J. Energy Chem.*, **2020**,**47**:172-179
- [35] Wu X, Liu N N, Guan B, Qiu Y, Wang M X, Cheng J H, Tian D, Fan L S, Zhang N Q, Sun K N. *Adv. Sci.*, **2019**,**6**(21):1900958
- [36] Wang S F, Hou X H, Zhong Z M, Shen K X, Zhang G Z, Yao L M, Chen F M. *Sci. Rep.*, **2018**,**8**(1):1-9
- [37] Chen T M, Shang Z C, Yuan B, Wu N X, Abuzara M, Yang J Y, Gu X X, Miao C Y, Ling M, Li S. *Energy Technol.*, **2020**,**8**(7):2000302
- [38] Feng X H, Wang Q, Li R R, Li H. *Appl. Surf. Sci.*, **2019**,**478**:341-346
- [39] Liang X, Rangom Y, Kwok C Y, Pang Q, Nazar L F. *Adv. Mater.*, **2017**,**29**:16030040-16030046
- [40] Deng J N, Guo J Q, Li J, Zeng M, Gong D Y. *Ceram. Int.*, **2018**,**44**(14):17340-17344
- [41] Wan T T, Liu S M, Evans K, Gerhardt A, Li J D, Liu G H, Zhang Z S. *Nanotechnology*, **2020**,**31**(26):265406
- [42] Dong W, Meng L Q, Hong X D, Liu S Z, Shen D, Xia Y K, Yang S B. *Molecules*, **2020**,**25**(8):1989
- [43] Lin C, Zhang W K, Wang L, Wang Z G, Zhao W, Duan W H, Zhao Z G, Liu B, Jin J. *J. Mater. Chem. A*, **2016**,**4**:5993-5998
- [44] Sun K, Cama C A, DeMayo R A, Bock D C, Tong X, Su D, Marschilok A C, Takeuchi K J, Takeuchi E S, Gan H. *J. Electrochem. Soc.*, **2017**,**164**:A6039-A6046
- [45] Zhang R, Rao Z G, Li Y, Li H Y, Fei L F, Lei S J, Wang Y. *ChemistrySelect*, **2019**,**4**(19):5678-5685